Microchimica Acta (2019) 186: 208
https://doi.org/10.1007/s00604-019-3330-z

ORIGINAL PAPER

Synthesis of poly(1,5-diaminonaphthalene) microparticles with abundant amino and imino groups as strong adsorbers for heavy metal ions

Xin-Gui Li[1,2,3,4] · Mei-Rong Huang[1,3,4] · Yuan-Bo Jiang[3] · Jie Yu[2] · Zikai He[2]

Received: 1 February 2019 / Accepted: 16 February 2019 / Published online: 2 March 2019

Abstract

Poly(1,5-diaminonaphthalene) microparticles with abundant reactive amino and imino groups on their surface were synthesized by one-step oxidative polymerization of 1,5-diaminonaphthalene using ammonium persulfate as the oxidant. The molecular, supramolecular, and morphological structures of the microparticles were systematically characterized by IR and UV-vis spectroscopies, elementary analysis, wide-angle X-ray diffractometry, and transmission electron microscopy. The microparticles demonstrate electrical semiconductivity and high resistance to strong acid and alkali, and strong adsorption capability for lead(II), mercury(II), and silver(I) ions. The experimental conditions for adsorption of Pb(II) were optimized by varying the persulfate/monomer ratio, adsorption time, sorbent concentration, and pH value of the Pb(II) solution. The maximum adsorption capacity is 241 $mg \cdot g^{-1}$ for particles after a 24 h-exposure to a solution at an initial Pb(II) concentration of 29 mM. The adsorption data fit a Langmuir isotherm and follow a pseudo-second-order reaction kinetics. This indicates a chemical adsorption that is typical for a chelation interaction between Pb(II) and amino/imino groups on the sorbent.

Keywords 1,5-diaminonaphthalene polymer · Oxidative polymerization · Particle adsorbent · Metal chelate · Lead ion removal · Mercury ion sorption · Silver recovery · Polyaniline derivative · Amino polycondensate · Water purification

Introduction

The adsorption of heavy metal ions is still facing big challenges due to the difficulty of simultaneously realizing strong adsorption and sustainable preparation of the adsorbents. Ideal adsorbents should have several crucial characteristics including a large specific surface area, strong water/acid/alkali resistance, environmental innocuousness, readily and sustainable preparation. Such sorbents also should possess many functional groups that can strongly and reversibly interact with

Electronic supplementary material The online version of this article (https://doi.org/10.1007/s00604-019-3330-z) contains supplementary material, which is available to authorized users.

✉ Xin-Gui Li
lixingui@tongji.edu.cn

✉ Mei-Rong Huang
huangmeirong@tongji.edu.cn

✉ Zikai He
hezikai@hit.edu.cn

[1] State Key Laboratory of Pollution Control and Resource Reuse, and Shanghai Institute of Pollution Control and Ecological Security, and International Joint Research Center for Sustainable Urban Water System, College of Environmental Science and Engineering, Tongji University, 1239 SiPing Road, Shanghai 200092, China

[2] Key Laboratory of Theory & Technology for Micro-Nano Optoelectronic Information System of Ministry of Industry & Information Technology, College of Materials Science and Engineering and School of Science, Harbin Institute of Technology (Shenzhen), Guangdong 518055, China

[3] Key Laboratory of Advanced Civil Engineering Materials, College of Materials Science and Engineering, Tongji University, Shanghai 200092, China

[4] Department of Molecular Engineering, Kyoto University, Nishikyo-ku, Kyoto 615-8510, Japan

the metal ions [1, 2]. It is reported that some thio-functionalized materials and porous modified silica seem to be two of powerful adsorbents [1–4]. An activated carbon based on potato peels exhibited the maximum Pb(II) adsorption capacity of 167 $mg \cdot g^{-1}$ [5]. The thiol-functionalized activated carbon and hybrid macroporous modified silica had the maximum Pb(II) sorption capacity of 238.1 $mg \cdot g^{-1}$ [3] and 256.7 $mg \cdot g^{-1}$ [4], respectively. A mesoporous silica-grafted graphene oxide (GO) can achieve the maximum Pb(II) adsorption capacity of up to 255.1 $mg \cdot g^{-1}$ within 10 min and also selectively adsorb more than 99% of Pb(II) ions in the presence of other metal ions [6]. Cross-linked melamine-based polyamine/CNT composites have a high removal efficacy of up to ~99% of Pb(II) ions in wastewater [7]. However, it should be noticed that thiolating agents (such as Na_2S, $HSCH_2COOH$, $(CH_3O)_3Si(CH_2)_3SH$, $HSCH_2CH_2SO_3H$, and $HS(CH_2)_3SO_3H$) and sophisticated multistep preparation procedures are generally required [1–4]. Moreover, sophisticated multistep procedures together with high-temperature carbonization or activation at up to 600~850 °C in an ultrapure (99.999% pure) inert atmosphere are also necessary for the preparation of the carbon-based adsorbents [5–7]. These consequently lead to new environmental polluted problems or low cost-efficacy because of the high toxicity and fetid odor of thiolating agents or lengthy and energy-consuming preparation process.

Fortunately, the above-mentioned problems can be avoided to some extent if choosing oxidative polymerization of ultra-low volatile aromatic diamines in aqueous reaction media at room temperature under an ambient air atmosphere for the one-stage direct preparation of the sorbents. In fact, as multifunctional organic conducting polymers, aromatic amino polymers have received much attention due to their straightforward preparation, unique properties and potentially wide applications including heavy metal ions adsorbents [8, 9] and noble metal recovery agent. As one of multifunctional oxidative polymers of aromatic diamines [8], poly(1,5-diaminonaphthalene) (P15DAN) should have great potential to serve as a rapid and efficient adsorbent to eliminate/recover heavy metal ions because of the existence of a large amount of $-NH_2$ amino/-NH- and -N = imino groups on its macromolecular chains. 1,5-Diaminonaphthalene (15DAN) not only has ultra-low vapor pressure of 2.3 μPa that is 565 million times lower than that of thioglycolic acid (1.3 kPa) but also oxidatively polymerizes into self-stabilized P15DAN nanoparticles at the interfaces between propylene carbonate and acid [10]. The formation mechanism and morphology, Cu(II) interaction, voltammetric response, colorful fluorescence emission, and Cu(II) and Zn(II) fluorescence detection of P15DAN nanoparticles have been elaborated [10]. The synthesis, high-resolution solid-state ^{13}C-NMR spectra, and Ag(I) sorption of the poly(1,8-diaminonaphthalene) (P18DAN) with 1,8-diaminonaphthalene as monomer has been reported [11]. However, the preparation, characterization, and Pb/Hg/Ag ion adsorbability of the microparticles by a homogeneous chemical oxidative polymerization of 15DAN in neutral acetonitrile/water solution without any acid have not been reported yet till now.

It has been demonstrated that heavy metal ions including Pb(II), Hg(II), and Ag(I) can readily be trapped by the P15DAN films via a complexation and also an ion-exchange between the metal ions and $–NH_2$/-NH–/-N = groups through sharing electron pairs on the N atoms [8, 10]. Obviously, P15DAN as a nonvolatile, harmless, and water–/acid–/alkali-resistant polymer can potentially be used for collection and removal of precious and hazardous heavy metal ions from water effluents without having to use any external energy source.

Therefore, we report a preliminary result on the productive one-step direct synthesis, structure and properties of P15DAN microparticles from water-insoluble 15DAN, especially on the powerful adsorption toward lead, mercury, and silver ions in the aqueous solution. The adsorption time, the ion concentration and pH were systematically optimized to reveal an appropriate adsorption condition of the metal ions onto the microparticles. The mechanism of the ion adsorption on the P15DAN is proposed for the first time.

Experimental

Reagents and materials: 1,5-diaminonaphthalene (15DAN) was purchased from Sigma-Alderich (https://www.sigmaaldrich.com). Ammonium persulfate (APS), ferric chloride ($FeCl_3$), acetonitrile, $Pb(NO_3)_2$, $Hg(NO_3)_2$, and $AgNO_3$ of analytical reagent grade were purchased from Sinopharm Chemical Reagent Co. Ltd. (Shanghai, China, http://www.sinoreagent.com). All of those reagents were used as received.

Synthesis of poly(1,5-diaminonaphthalene) microparticles: P15DAN microparticles were synthesized by a chemically oxidative polymerization of 15DAN in acetonitrile/water solution by using APS and $FeCl_3$ as oxidants, respectively. As a typical procedure,

1) 15DAN (0.79 g, 5 mmol) monomer solution in acetonitrile (50 mL) in a 200 mL glass flask at 20 °C was prepared;
2) the Pt working and SCE reference electrodes connected to a pH meter were inserted into the 15DAN (0.79 g, 5 mmol) solution;

3) APS (1.14 g, 5 mmol) aqueous solution (50 mL) was prepared and then added dropwise at a rate of one drop (60 μL) every 3 s to the 15DAN monomer solution in acetonitrile at 20 °C with continuously stirring;
4) Once the APS solution was added, the open-circuit potential was intermediately followed by a technique of open-circuit potential that is the potential at which there is no current. The open-circuit potential refers to the potential difference between the working and reference electrodes in the reaction solution system, which was recorded by a pH meter. The open-circuit potential can be used to reflect the variation of the concentration of the oxidants and reductants in the polymerization solution system.
5) The reaction mixture was constantly and vigorously stirred for 24 h at 20 °C;
6) The resulting polymer precipitates were filtered and washed thoroughly with distilled water to remove the residual oxidant and water-soluble oligomers.
7) Finally, the solid powders were dried for 3 days in ambient air at 40 °C until a constant mass was reached. Nominal one-step directly chemical oxidative polymerization of 15DAN in acetonitrile/water solution with ammonium persulfate as oxidants for the synthesis of P15DAN microparticles is shown in Scheme 1.

Characterization of structure and properties: The infrared (IR) spectra were recorded on Nicolet Magna 550 FT-IR Spectrometer made in USA at 2 cm^{-1} resolution on KBr pellets. UV-vis absorption spectra were measured on a Hitachi U-3000 Spectrophotometer made in Japan in a wavelength range of 290–900 nm with a 20 $mg{\cdot}L^{-1}$ homogeneous solution of the P15DAN in DMSO. The elemental analysis experiments were carried out on a Carlo Erba 1106 Element Analyzer. Wide-angle X-ray diffraction was performed with a Bruker D8 Advance X-ray Diffractometer made in Germany with Cu Kα radiation at a scanning rate of 0.89° min^{-1}. The morphology of the particles was observed by an H-800 Hitachi transmission electron microscope (TEM) by dropping a water suspension of the virgin particles onto a copper network. The bulk electrical conductivity of the microparticles was measured by a two-disk method using a UT 70A multimeter at ambient temperature. The solubility of the microparticles was evaluated by adding P15DAN powders of 5 mg into the solvent of 1 mL and dispersing thoroughly for 24 h at room temperature.

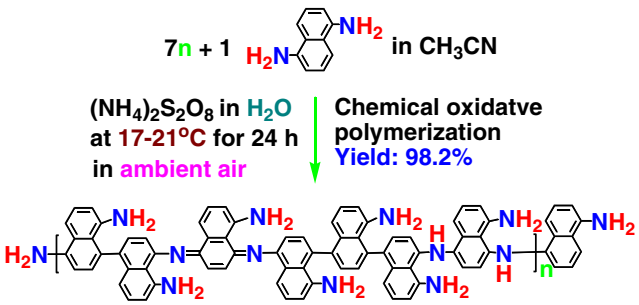

Scheme 1 Nominal chemically oxidative polymerization of 1,5-diaminonaphthalene (15DAN) in acetonitrile/water solution with ammonium persulfate as oxidant

Adsorption of heavy metal ions: Adsorption of Pb^{2+}, Hg^{2+} or Ag^{+} ions onto the P15DAN microparticles was performed in batch experiments. For batch tests, a given amount of particles was added into 25 mL $Pb(NO_3)_2$, $Hg(NO_3)_2$ or $AgNO_3$ aqueous solution at 30 °C. After a desired treatment period, the microparticles were filtered from the aqueous solution. The concentration of the metal ions in the filtrate was measured by a chemical titrimetric analysis [12] at a residual ion concentration of higher than 50 $mg{\cdot}L^{-1}$ or inductively coupled plasma (ICP) at a residual ion concentration of lower than 50 $mg{\cdot}L^{-1}$. The adsorbed amount of the ions on the particles was calculated [11, 12]. The number of repetitive experiments for metal-ion adsorption onto the microparticles is 3.

Results and discussion

Synthesis of poly(1,5-diaminonaphthalene) (P15DAN) microparticles: The chemical oxidative polymerization of 15DAN with APS or $FeCl_3$ as oxidants in acetonitrile/water solution simply affords black and uniform microparticles as synthetic products. Progress in the polymerization reaction has been in-situ followed by testing the solution temperature and potential. With slowly and regularly dropping the oxidant solution, the polymerization solution turns black accompanied by a sudden temperature fall from 20.0 to 17.1 °C for an initial 1 min of the reaction (Fig. 1a). This phenomenon is opposite to the chemical oxidative polymerization of 1,8-diaminonaphthalene (18DAN) [11], indicating that more energy is required to oxidize 15DAN monomer to radical cation for the polymerization. The oxidation potential of 15DAN monomer (0.58 V) is higher than that of 18DAN (0.41 V). With further dropping oxidant solution, the solution temperature increases gradually, and finally reaches a nearly constant value. This suggests that the polymerization is initially endothermic and then traditionally exothermic. The polymerization rate is not constant but self-accelerated, depending on the oxidant species and oxidant/15DAN ratio. Note that the polymerization at the oxidant/15DAN ratio of 2/1 is the most strongly endothermic due to the fastest reaction rate.

The variation of the reaction solution potential may provide a deeper insight into polymerization process. It is found that there are three district stages in the potential-time profile. After the oxidant solution was initially dropped to the

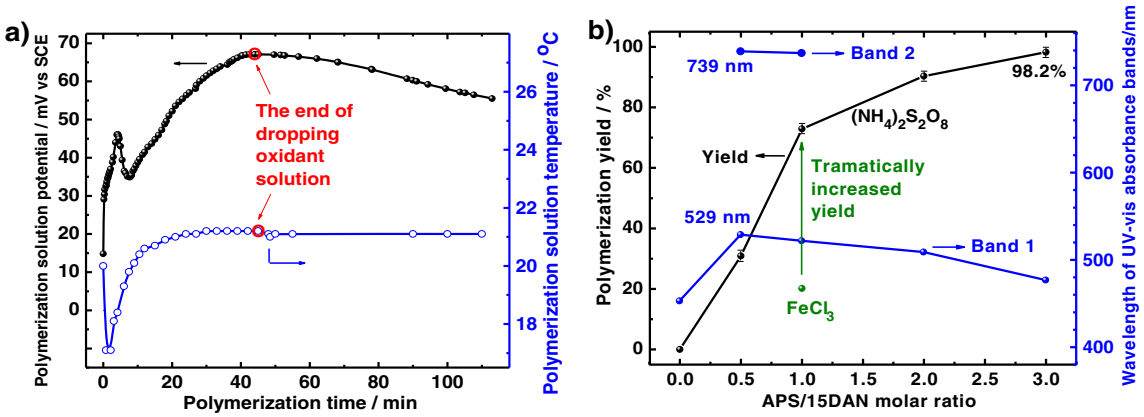

Fig. 1 **a** Typical plots of the solution potential and temperature with polymerization time at APS/15DAN molar ratio 1/1 in CH_3CN/H_2O. b) Polymerization yield and maximal UV-vis absorbance wavelength of the P15DAN microparticles with increasing APS/15DAN ratio from 0.5 to 3.0

15DAN solution, an immediate rise of potential was recorded. This drastic potential rise in initial polymerization time of 5 min is ascribed to dissociation of the persulfate ions into radical anions in the presence of the 15DAN monomer and subsequently the formation of oligomers. As the reaction proceeds, the potential gradually reaches the second maximum in 40 min, signifying the formation of P15DAN. In the third stage, the potential declines slowly and continually from the maximum potentials in 2 h, but it would not fall back to the initial potential because of the change of solution composition. The three stages indicate that the polymerization proceeds unsteadily and is autoaccelerated. As seen in Table 1, the 1st potential rise and the time at the 1st maximal potential both show a maximum at the APS/15DAN molar ratio of 1/1, indicating the slowest polymerization that is confirmed by the longest time at the minimal temperature among five APS/15DAN ratios. The polymerization with higher APS/15DAN ratio takes less time to reach a maximum potential, which suggests more polymerization active sites because more 15DAN monomers can be more easily oxidized to radical cations.

Therefore, the polymerization yield also depends remarkably on the oxidant species and APS/15DAN ratio (Fig. 1b). The APS with higher standard reduction potential of 2.01 V provides much higher yield than $FeCl_3$ with lower potential of 0.77 V. The yield increases monotonically and significantly from 30.9 to 98.2% as the APS/15DAN molar ratio rises from 1/2 (0.5) to 3/1 (3.0), because more oxidant will produce more active sites for polymerization.

Structure of poly(1,5-diaminonaphthalene) (P15DAN) microparticles: IR, UV-vis, elemental analysis, wide-angle X-ray diffraction, and TEM have all been used to analyze the structure characteristics of the microparticles. A very pronounced change of the IR spectral characteristics is observed before and after the chemical oxidative polymerization with increasing APS/15DAN molar ratio from 0/1 to 3/1(Fig. 2a). The IR spectrum of 15DAN monomer at 3400 and 1600 cm^{-1} due to amino and naphthylene units is quite different from the spectra of the P15DAN products at four APS/15DAN ratios of 1/2 to 3/1. Three absorption bands at 3200, 3300 and 3400 cm^{-1} due to symmetric and asymmetric $–NH_2$ stretching vibrations of 15DAN monomer merge into a broad band centered at 3433 cm^{-1} for the products. Two bands at 1629 and 1521 cm^{-1} due to naphthylene rings of 15DAN monomer also merge into an overlapped doublet centered at 1600 for the products. Particularly, a strong shoulder peak at 1650 cm^{-1} is associated with the stretching of the C=C and C=N bonds on quinoid rings. The P15DAN at APS/DAN molar ratios between 1/1 and 3/1 demonstrates stronger absorbance at

Table 1 The variation of the temperature and potential of polymerization solution with APS/15DAN molar ratios in CH_3CN/H_2O at initial 20 °C

APS/15DAN molar ratio	Polymerization solution temperature (°C)			Solution potential (mV vs. SCE)		
	Minimal temperature[a]	Temperature fall	Time at minimal temperature (min)	Initial / maximal potential	Potential rise	Time at maximal potential (min)
1/2	18.2	1.8	2.0	11/278;233	267;222	1.5;42
1/1	17.1	2.9	2.2	148/461;671	313;523	4.2;43
2/1	17.0	3.0	0.52	55/295;690	240;635	1.2;140
3/1	17.4	2.6	1.0	55/289;690	234;635	0.3;153
1($FeCl_3$)/1	14.5	5.5	2.5	25/189;235	164;210	0.6;16.4

[a] The initial temperature of polymerization solution was fixed at 20 °C

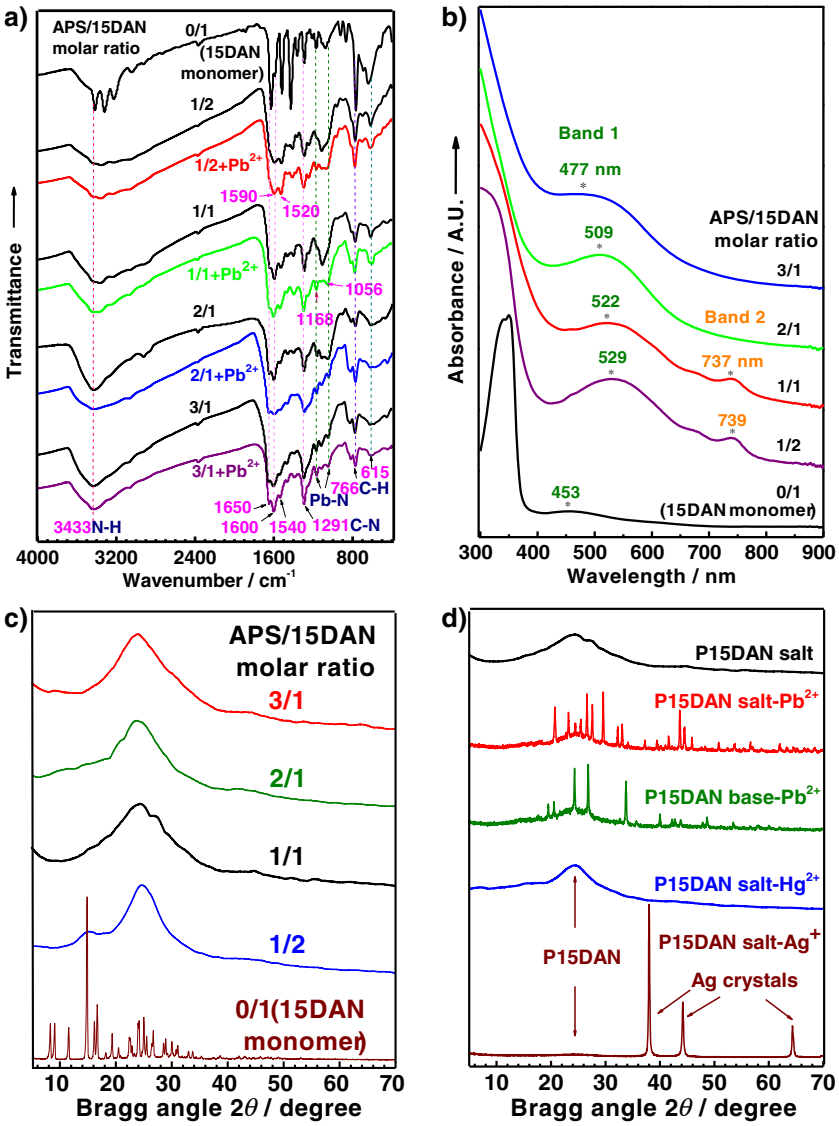

Fig. 2 **a** IR spectra before and after lead-ion adsorption and **b**) UV-vis spectra of the DMSO solution at a concentration of 20 mg·L^{-1} of 15DAN and P15DAN prepared at various APS/15DAN feed molar ratios. Wide-angle X-ray diffractograms of **c)** P15DAN salt microparticles prepared at different APS/15DAN ratios and **d)** lead, mercury and silver ions-adsorbing P15DAN salt/base microparticles prepared at APS/15DAN molar ratio of 1/1

1600–1650 cm^{-1} and weaker absorbance at 1520–1540 cm^{-1} than that at the APS/DAN molar ratio of 1/2. This indicates overoxidation of the P15DAN by more oxidant. The C-N stretching band at 1291 cm^{-1} of 15DAN monomer is much weaker than that of the products at four APS/15DAN molar ratios of 1/2 to 3/1. On the contrary, the C-H stretching and bending bands at 766 and 615 cm^{-1} of 15DAN monomer are stronger than those of the products. That is to say, the formation of the secondary N-H and C=N bonds, the increase of C-N bond content but the decrease of C-H bond content all imply that the oxidative polymerization proceeds through the formation of C-NH-C and C=N-C bridge bonds, i.e., the formation of a real polymer. Especially, only the P15DAN formed at the APS/15DAN ratio of 1/2 exhibits two distinct IR absorptions with equivalent intensity at 1590 and 1520 cm^{-1} that correspond to quinoid and benzenoid rings respectively. This IR spectral characteristics is similar to that of highly conducting polyaniline with a typical large π-conjugated structure, signifying that the P15DAN has a similar main chain structure like polyaniline.

Similarly, a great UV-vis spectral difference between 15DAN monomer and P15DAN bases has been revealed (Fig. 2b). Four P15DANs show a strong absorbance peak around 300 nm assigned to π-π* transition from the benzenoid ring and a broad absorbance peak at 477–529 nm assigned to n-π* excitation band or interband charge transfer that is associated with the excitation of benzenoid to quinoid rings. With increasing APS content, the absorbance around 477–529 nm rises steadily, indicating an increased concentration of the quinoid units. Especially, the P15DANs at two APS/15DAN ratios of 1/2 and 1/1 exhibit an additional small absorbance at the wavelength of 739 and 737 nm (Figs. 1b and 2b), indicating that the both polymers have even larger π-conjugated structure than other two. In particular, the.

P15DAN formed at the APS/15DAN ratio of 1/2 displays the two absorbance bands at the longest wavelength at 529 and 739 nm, suggesting the longest π-conjugated length. This is coincided with the results of above-mentioned equivalent IR absorptions at 1590 and 1520 cm^{-1} and their highest electrical conductivity discussed below. The elemental composition and chain structure of P15DANs are listed in Table S1. The molecular structure varies remarkably with APS/15DAN ratio from 1/1 to 2/1. Obviously, a denitrogenation during the oxidative polymerization of 15DAN becomes stronger at higher oxidant content, like the denitrogenation phenomenon during the chemical oxidative polymerization of 18DAN [11]. Excrescent experimental H content in the P15DAN must be ascribed to the presence of the water trapped firmly in P15DAN. It appears that the π-conjugated structure is better in P15DAN(1/1) than P15DAN(2/1), which is confirmed by UV-vis spectra and a relatively high electrical conductivity of the former in Table S2. In particular, there are more amino(-NH_2) groups in P15DAN(1/1) than P15DAN(2/1), which is coincident with much stronger Ag^+ adsorbability of the former, as discussed below.

The wide-angle X-ray diffractograms of P15DAN microparticles are shown in Fig. 2c. Unlike crystalline 15DAN monomer, four P15DAN particles are all amorphous, signifying that they are real polymers. They exhibit a broad diffraction peak centered at a Bragg angle of 25°, and their diffraction characteristics vary slightly with APS/15DAN molar ratio. The TEM images in Fig. S1 reveal that the dried P15DAN salts particles have irregular shape and rugged surface, and the size ranging from 600 to 4500 nm. Here, 41 different particles shown in TEM images have been taken into account to estimate the particle size. The amorphous, irregular, rugged and small particles are advantageous to their full interaction toward the metal ions to achieve a high ion adsorbability [13].

Properties of poly(1,5-diaminonaphthalene) (P15DAN) microparticles: Table S2 summarizes the conductivity, solubility and solution color of the P15DAN microparticles with different APS oxidant/15DAN ratios. Two P15DANs synthesized at APS/15DAN molar ratios of 1/2 and 1/1 have higher electrical conductivity than those synthesized at APS/15DAN molar ratios of 2/1 and 3/1 and $FeCl_3$/15DAN molar ratio of 1/1. In particular, the P15DAN formed at the APS/15DAN molar ratio of 1/2 has the highest electrical conductivity, which has been confirmed by the equivalent IR absorptions at 1590 and 1520 cm^{-1} and the longest wavelength at 529 and 739 nm of UV-vis absorbances in Figs. 2a,b. The 15DAN monomer and five P15DANs are all soluble in high polar organic solvents like NMP, DMSO, and DMF and mainly soluble in THF. The solutions of P15DANs look dark red in NMP, DMSO, and DMF and red in THF. All of these indicate that the P15DANs have potential solution processibility. Note that the P15DANs formed with APS oxidant are mainly soluble in some common organic solvents like THF but completely insoluble in H_2O, HCl and NaOH aqueous solutions. In other words, the P15DANs exhibit much higher insolubility or resistance to strong acid or alkali aqueous media than organic solvents. The P15DAN particles by $FeCl_3$ are partly soluble in aqueous acid and alkali and water. This indirectly verifies that the P15DAN particles by APS have higher molecular weight or higher resistance to acid, alkali and water than those by $FeCl_3$. All of these imply that the P15DANs produced by APS are real polymers and also appropriate for the elimination and recovery of heavy and noble metal ions even in the wastewater containing acid and alkali.

Selective adsorption and its mechanism of Pb^{2+}/Hg^{2+}/Ag^+ ions onto P15DAN microparticles: The microparticles exhibit dramatically variable metal-ion adsorbability, depending on ion species and APS/15DAN ratio used, as summarized in Table 2. With changing APS/15DAN molar ratio from 0/1 to 3/1, the Ag^+ adsorbability declines significantly, the Pb^{2+} adsorbability illustrates a maximum at APS/15DAN molar ratio of 1/1, but the Hg^{2+} adsorbability fluctuates in a narrow range between 72 and 94 $mg{\cdot}g^{-1}$. Particularly, the Pb^{2+} adsorbability is always the lowest, while the Ag^+ adsorbability is generally the highest except for the P15DAN(3/1). However, the Ag^+ adsorbability is still lower than that onto the P18DAN microparticles [11], because of the presence of many more -NH_2 groups in the P18DAN macromolecular chains. Similarly, it has been confirmed in our laboratory that the Hg^{2+} adsorbability is also lower than that onto the P18DAN microparticles. It should be noted that the Pb^{2+} adsorbability is actually stronger than that onto the P18DAN microparticles. This huge difference of the metal ions on both types of isomeric polymer microparticles must be ascribed to quite distinct adsorption mechanism, i.e., the chelation adsorption of Pb^{2+} and the redox adsorption of Ag^+, as elaborated below. It is concluded that the adsorption capacity of three heavy-metal ions onto the P15DAN microparticles can be ranked in an increasing order below:

$$Pb^{2+} < Hg^{2+} < Ag^+$$

The adsorptivity of three heavy-metal ions onto the P15DAN microparticles can be ranked in an increasing order below:

$$Ag^+ < Pb^{2+} < Hg^{2+}$$

The selective or competitive adsorption of the heavy metal ions onto the particles over common nontoxic metal ions including Na(I), K(I), Ca(II), and Mg(II) ions in real-world samples at a higher excess has also been briefly investigated. It is found that the P15DAN particles demonstrate much stronger adsorbability toward Ag(I), Hg(II), and Pb(II) ions than relatively light Na(I), K(I), Ca(II), and Mg(II) ions

Table 2 The adsorption of heavy metal ions onto the poly(1,5-diaminonaphthalene) (P15DAN) salt particles synthesized by a chemically oxidative polymerization with the particle adsorbent dosage of 50 mg in 25 mL ion solution at an initial Pb^{2+} {or Hg^{2+}} concentration of 200 $mg{\cdot}L^{-1}$ and an initial Ag^{+} concentration of 10.044 $g{\cdot}L^{-1}$ at 30 °C for 24 h

APS/15DAN molar ratio	Adsorption capacity ($mg{\cdot}g^{-1}$)			Adsorptivity (%)		
	Pb^{2+}	Hg^{2+}	Ag^{+}	Pb^{2+}	Hg^{2+}	Ag^{+}
0/1 (15DAN monomer)	0(16 ± 0.5)[a]	94 ± 2.8 (474 ± 2.9)[a]	1975 ± 2.5[b]	0(16 ± 0.5)[a]	94 ± 2.8 (97 ± 2.9)[a]	84 ± 2.5[b]
1/2	72 ± 2.2(38 ± 1.1)[c]	72 ± 2.3	522 ± 0.3	72 ± 2.2 (38 ± 1.1)[c]	72 ± 2.3	11 ± 0.3
1/1	81 ± 2.4(66 ± 2.0)[c]	91 ± 2.7	680 ± 0.4	81 ± 2.4(66 ± 2.0)[c]	91 ± 2.7	14 ± 0.4
2/1	48 ± 1.4	83 ± 2.5	110 ± 0.1	48 ± 1.4	83 ± 2.5	2.2 ± 0.1
3/1	14 ± 0.4	82 ± 2.5	33 ± 0.02	14 ± 0.4	82 ± 2.5	0.65 ± 0.02

[a] Onto 18DAN monomer at initial Hg^{2+} concentration of 979 $mg{\cdot}L^{-1}$

[b] Onto 15DAN monomer at initial Ag^{+} concentration of 4.644 $g{\cdot}L^{-1}$

[c] Onto the dedoped P15DAN base particles

because of the much stronger complexation interaction between the heavy metal ions and P15DAN molecules [14]. Therefore, the particles are useful to efficiently and selectively extract Ag(I), Hg(II), and Pb(II) from their mixture including real-world polluted water and wastwaters with Na(I), K(I), Ca(II), and Mg(II) ions, accomplishing proper decontamination of toxic heavy metals.

Note that it has been discovered that the aniline/sulfoanisidine copolymer nanosorbents have demonstrated even both higher adsorption capacity and higher adsorptivity of Hg^{2+} ions [15] than the P15DAN microparticles. Therefore, the P15DAN microparticles are not the strongest adsorbent toward Hg^{2+}, but they are the most appropriate for Pb^{2+} adsorption because of a combination of high Pb^{2+} adsorptivity, low cost and good insolubility in water, acidic, and alkaline solutions. Detailed optimization of adsorption conditions of Pb^{2+} will be performed in the following section.

Generally, the main adsorption sites for heavy metal ions locate between the = N-, -NH- and $-NH_2$ groups in the macromolecular chains because three types of nitrogen atoms all have a lone pair of electrons that can efficiently bind a metal ion through sharing an electron pair to form a metal complex. However, the preference of three ions towards the three nitrogen atoms is dissimilar. For example, Pb^{2+} would not allow a ligand-to-metal charge transfer complex to be formed due to the Pb^{2+} electronic configuration of $4f^{14}5d^{10}6s^{2}6p^{0}$, which is confirmed by the fact that the 15DAN monomer with a lot of isolated amino($-NH_2$) groups each other has no adsorbability to lead ions. Lead ion can form a stable chelation with N between amino and imino groups, a six-membered heterocyclic chelating ring. It has been known for many years that the complex resulting from coordination with the chelating ligand is much more thermodynamically stable. It is also known that there should be some $-NH_3^{+}$ groups on the chain structure of the P5DAN particles formed in acidic and neutral aqueous solution. Therefore, another possible approach of the Pb^{2+} adsorption is ion exchange between Pb^{2+} and H^{+} on the $-NH_3^{+}$. This has been proved by the fact that the final pH value of the resultant $Pb(NO_3)_2$ solution after Pb^{2+} adsorption onto the P15DAN salt particles is lower than the initial pH value (Table 3). These indicate that some H^{+} ions are released into the solution as the Pb^{2+} ions are bound onto the particles. On the other hand, slightly increased pH value of the Pb^{2+} solution after the Pb^{2+} adsorption onto P15DAN base particles without H^{+} also indirectly verifies above-mentioned ion exchange. As discussed below, the adsorption capacity is only slightly influenced by the pH, suggesting that the ion exchange plays a minor role in the adsorption. In fact, the maximum adsorption amount of the ion exchange only accounts for 4.07% of total adsorption capacity. In addition, the Pb^{2+} can also be weakly bound to the P15DAN particles in physical adsorption by van der Waals force. It is reported that electrosynthesized P15DAN merely has a physical adsorption with a low adsorption efficiency of one Pb^{2+} on every 31 15DAN units, whereas the total adsorption efficiency is one Pb^{2+} on every 5.3 15DAN units. This means that the physical adsorption should not be the main mechanism for the Pb^{2+} adsorption. In summary, the chelation may be dominant during the Pb^{2+} adsorption.

On these considerations, possible adsorption mechanisms by chelation, complexation, redox, and ion exchange between

Table 3 The solution pH before and after Pb^{2+} adsorption in 25 mL solution at Pb^{2+} concentration of 200 $mg{\cdot}L^{-1}$ with poly(1,5-diaminonaphthalene) (P15DAN) salt particle dosage of 50 mg at 30 °C for 24 h

Adsorbent	APS/15DAN molar ratio	Adsorbed solution		
		Initial pH	Final pH	ΔpH
P15DAN salt	1/1	5.1	4.4	−0.7
P15DAN salt	1/2	5.1	4.6	−0.5
P15DAN base	1/2	5.1	5.4	0.3

the metal ions and the P15DAN chains may be displayed in Scheme 2. On the basis of the adsorption mechanism, theoretically every two chains of P15DAN($n = 1$) should chelate 3 lead ions, so the maximum Pb^{2+} adsorption capacity of P15DAN(n = 1) should be 256 $mg{\cdot}g^{-1}$, which is slightly lower than simulatively maximal adsorption capacity (265.3 $mg{\cdot}g^{-1}$ in Table 4) but slightly higher than experimentally maximal Pb^{2+} adsorption capacity (241.0 $mg{\cdot}g^{-1}$) in Fig. 3b.

In the IR spectra of all the chelates, two new medium intensity bands at 1168 and 1051 cm^{-1} assignable to Pb-N vibration (Fig. 2a), which are nearly absent in the Pb^{2+}-free polymers, suggest that Pb^{2+} ions have been chelated onto the polymers. This information is very similar to the IR spectra of other Pb^{2+} complexes [16].

The occurrence of the metal-ion adsorption onto the P15DAN microparticles has been further confirmed by the variation of the X-ray diffraction of the microparticles with Pb^{2+} adsorption. The P15DAN particles adsorbing Pb^{2+}/Ag^{+} ions exhibit a series of new sharp diffraction peaks in Fig. 2d as compared with the original polymers, but the P15DAN particles adsorbing Hg^{2+} ions do not exhibit any sharp diffraction peaks. The characteristic diffraction peaks of the P15DAN salt adsorbing Pb^{2+} indicate the presence of $PbSO_4$ from a reaction between Pb^{2+} and SO_4^{2-} rather than $Pb(NO_3)_2$, suggesting a reactive adsorption of Pb^{2+} on the particles. The SO_4^{2-} should result from residual free sulfate and doping sulfuric acid in the particles when APS is used as oxidant. Differently, no diffraction peak from $PbSO_4$ crystal is observed for the P15DAN base adsorbing Pb^{2+}, but the diffraction characteristics of $PbCO_3$ crystals are discovered, which may be caused by the CO_2 from the air. The P15DAN base prepared after dedoping process has relatively weak Pb^{2+} adsorbability as compared with P15DAN salt (Table 2). $PbSO_4$ and the $PbCO_3$ chemical depositions contribute 18.7 and 5.7% to the total Pb^{2+} adsorption capacity on P15DAN salt and base, respectively.

Note that the particles adsorbing 91 mg Hg^{2+} per gram of the particles do not exhibit any crystalline peak (Fig. 2d),

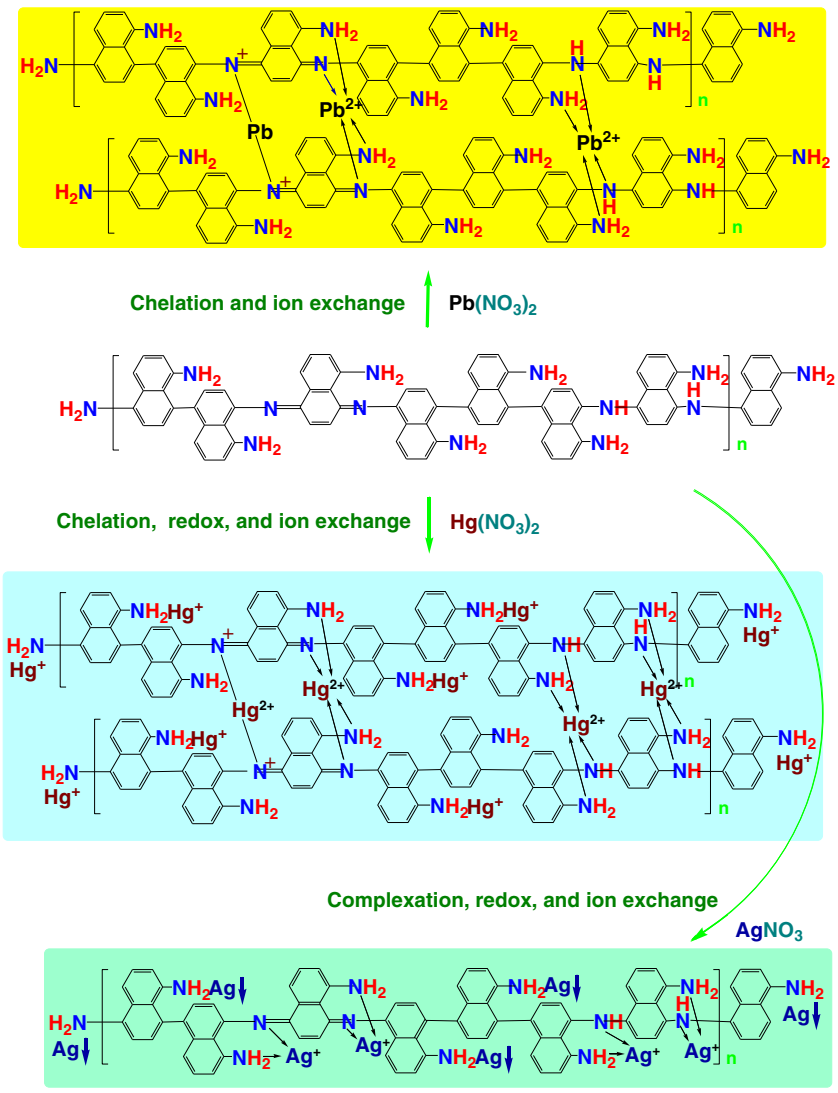

Scheme 2 Chelation, complexation, redox, and ion exchange between $Pb^{2+}/Hg^{2+}/Ag^{+}$ ions and amino/imino groups on the macromolecular chains of the P15DAN at APS/15DAN molar ratio of 1/1

Table 4 Isotherm model equations for Pb^{2+} adsorption onto P15DAN particles based on the data in Fig. 3

Isotherm model	Equation	Correlation coefficient	Standard deviation	Saturated adsorption capacity Q_m ($mg \cdot g^{-1}$)
Langmuir	$Q_e = 47797C_e / (180C_e+1)$	0.9852	1.0711	265.3
Freundlich	$Q_e = e^{6.59} C_e^{0.347}$	0.9778	0.1156	
Temkim	$Q_e = 357.3 + 42.92 \ LnC_e$	0.9518	21.4542	

signifying that the Hg^{2+} adsorption onto the particles results from the complexation between Hg^{2+} and macromolecular chains. However, the complexation and precipitation adsorptions of Pb^{2+} and Ag^{+} onto the particles occur simultaneously.

A high adsorbability of Ag^{+} onto P15DAN(1/1) microparticles (Table 2) is again confirmed by three strong sharp diffraction peaks at 38°, 44° and 64° (Fig. 2d) corresponding to the diffraction of lattice planes of Ag crystals. In fact, besides the complexation of Ag^{+} with $-NH_2$/-NH−/-N = groups, some Ag^{+} can immediately be reduced to elementary Ag by $-NH_2$/-NH- groups after it is adsorbed onto the P15DAN particles. It is also reported that electrosynthesized P15DAN can be oxidized by Ag^{+}.[17] By the way, the lowest adsorbability of Ag^{+} onto the P15DAN formed at APS/15DAN molar ratio of 3/1 should be attributable to the least $-NH_2$/-NH- groups because most of $-NH_2$/-NH- groups have been overoxidized into -N = groups by the excessive APS.

Optimized adsorption of Pb^{2+} ions onto P15DAN particles: The Pb^{2+} adsorbability is strongly influenced by the APS/15DAN ratio and Pb^{2+} concentration (Fig. 3), which can be used to optimize adsorption conditions of Pb^{2+} ions onto P15DAN particles. The P15DAN (1/1) has much higher adsorbance and adsorptivity of Pb^{2+} ions than P15DAN (2/1 and 3/1) in the same initial Pb^{2+} concentration range between 200 and 1000 $mg \cdot L^{-1}$ because there are more $-NH_2$/-NH- and $-NH_2$/-N = couples in P15DAN (1/1) chains (Table S1). With increasing initial Pb^{2+} concentration from 0 to 1000 $mg \cdot L^{-1}$, Pb^{2+} adsorbance monotonically rises but the Pb^{2+} adsorptivity declines. It seems that the microparticles demonstrate an optimal combination of high Pb^{2+} adsorbance and high adsorptivity at an initial Pb^{2+} concentration of 200 $mg \cdot L^{-1}$. The P15DAN(1/1) possessing the balanced strongest Pb^{2+} adsorbability at an initial Pb^{2+} concentration of 200 $mg \cdot L^{-1}$ is selected for the following detailed investigation. Note that the P15DAN particles demonstrate an increased Pb(II) adsorptivity from 81.4 to 87.0% with decreasing Pb(II) concentration from 200 to 100 $mg \cdot L^{-1}$. This indicates that the extracting ability would be stronger at a lower Pb(II) concentration. In fact, the P15DAN particles would be used to extract the Pb(II) ions at a low concentration down to ca 5 $mg \cdot L^{-1}$. This has been suggested by the longan shell adsorbent that has similar Pb(II) adsorptivity to P15DAN particles in the same dilute concentration [14].

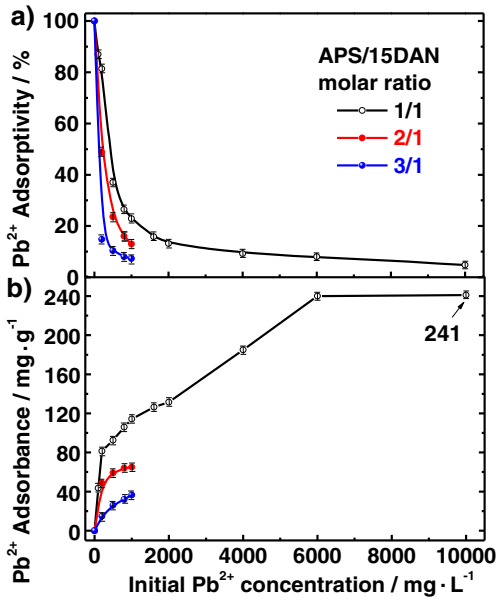

Fig. 3 Effect of initial Pb^{2+} concentration and APS/15DAN ratio on Pb^{2+} adsorbability onto P15DAN microparticles

Adsorption kinetics of Pb^{2+} ions on P15DAN particles: The time course experiments were carried out in order to analyze Pb^{2+} content at a certain contact time. Adsorption kinetics is studied to determine the time required for reaching equilibrium adsorption of Pb^{2+} ions. Figure 4 shows the profiles of Pb^{2+} adsorption capacity and adsorptivity versus adsorption time on the P15DAN particles. Apparently, the adsorbance and adsorptivity of Pb^{2+} increase non-linearly with the adsorption time. The adsorption process consists of two steps: a primary rapid step and a secondary slow step. The rapid step lasts for about 1 h and accounts for approximately 98% in the total Pb^{2+} adsorption, while the secondary step contributes to a negligible effect on the amount of adsorption. The fast step of Pb^{2+} adsorption may occur on the particle surfaces due to a fast chelation between Pb^{2+} and the amino/imino groups in the P15DAN chains, while the slow step might occur inside the particles, representing the diffusion of Pb^{2+} ions into inner of the P15DAN particles over the period. It is concluded that the cost-effective adsorption time would be 1 h.

A study on adsorption kinetics provides valuable insight into the pathways and mechanism of adsorption reaction. In addition, the kinetics can be used to describe the Pb^{2+} adsorption rate that in turn controls the residence time of sorbate uptake at the solid-solution interface. The experimental data

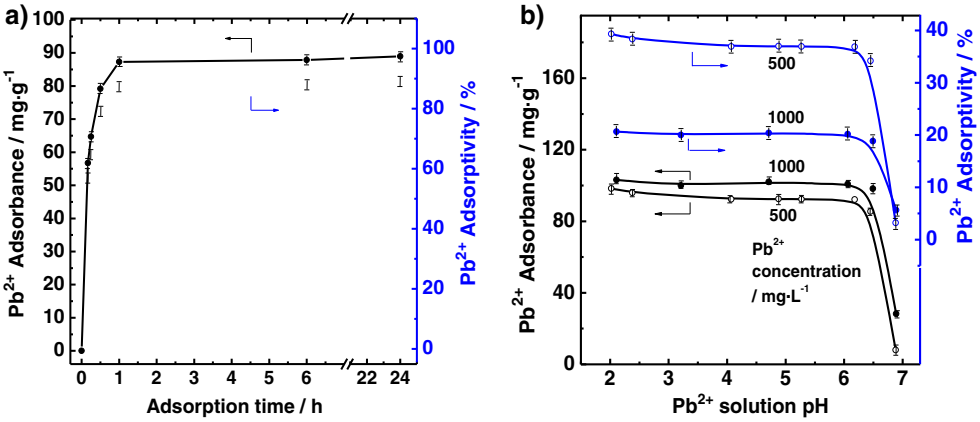

Fig. 4 Effect of **a**) adsorption time at initial Pb^{2+} concentration of 200 mg·L^{-1} and **b**) initial solution pH at two initial Pb^{2+} concentrations of 500 and 1000 mg·L^{-1} for 24 h on Pb^{2+} adsorbability onto P15DAN particles in 25 mL $Pb(NO_3)_2$ solution at 30 °C with particles dosage of 50 mg

were fitted into the kinetic equations of Lagergren, pseudo-first-order and pseudo-second-order. Their adsorption-rate expressions are as follows:

$$-\mathrm{Ln}\,(1-F) = k\,t \qquad \text{(Lagergren)} \qquad (1)$$

Where F equals Q_e/Q_t, Q_e the amount adsorbed (mg·g^{-1}) at equilibrium, Q_t the amount adsorbed (mg·g^{-1}) at time t, and k the adsorption-rate constant (h^{-1}).

$$t/Q_t = (t/Q_e) + (1/h') \qquad \text{(pseudo-second-order)} \qquad (2)$$

$$\mathrm{Log}\,(Q_e - Q_t) = \mathrm{Log}\,Q_e - k' t/2.303 \qquad \text{(pseudo-first-order)} \qquad (3)$$

Where the k' is the rate constant of pseudo-first-order adsorption (min^{-1}) and h' the initial adsorption rate of pseudo-second-order adsorption (mg·g^{-1}·min^{-1}). It is found that the application of pseudo-second-order model provides better correlation of the experimental data than the pseudo-first-order and Lagergren models (Table 5). Additionally, the equilibrium adsorbance determined using the pseudo-first-order model gives much lower value than experimentally determined value. It thus appears that the system under study is more appropriately described by the pseudo-second-order model based on the assumption that the rate limiting step may be chemisorption involving valency forces through sharing or exchange of electron between adsorbent and adsorbate [9, 11, 14, 15].

Effect of initial Pb^{2+} concentration and adsorption isotherm: The effect of the initial Pb^{2+} concentration on the equilibrium adsorption for 24 h has been investigated. The adsorption of Pb^{2+} ions on P15DAN(1/1) particles is given as a function of initial Pb^{2+} concentration in Fig. 3. Just like most other adsorbents [4], the Pb^{2+} adsorptivity decreases with an increase in Pb^{2+} concentration but the adsorbance rises significantly up to 240 and 241 mg·g^{-1} at the Pb^{2+} concentration of 6 and 10 g·L^{-1}, respectively. The elevated Pb^{2+} adsorbance on P15DAN with increasing Pb^{2+} concentration must be attributed to a greater probability of collision between Pb^{2+} and P15DAN particles, as well as also the full use of the adsorbing sites on the particles.

To quantitatively establish the relationship between Pb^{2+} concentration and adsorption process, three linearized mathematical models by Langmuir, Freundlich and Temkin are used to describe and analyze the adsorption isotherm and equilibrium, as listed in the following equations:

$$C_e/Q_e = (C_e/Q_m) + [1/(K_a Q_m)] \qquad (4)$$

$$\mathrm{Log}\,Q_e = (1/n)\,\mathrm{Log}\,C_e + \mathrm{Log}\,K_F \qquad (5)$$

$$Q_e = K_1 \mathrm{Ln}\,K_2 + K_1 \mathrm{Ln}\,C_e \qquad (6)$$

where C_e is the equilibrium Pb^{2+} concentration (M), Q_m the maximum adsorption capacity of the system (mg·g^{-1}), K_a the adsorption coefficient related to the energy of the adsorption (L·mg^{-1}), K_F, K_1, K_2 the equilibrium constants indicating adsorption capacity, and n adsorption equilibrium constant. The values of these constants are evaluated from the intercept and the slope, respectively, of the linear plots of C_e/Q_e vs. C_e, Q_e vs. Ln C_e and Log Q_e vs. Log C_e, based on experimental

Table 5 Kinetic model equations for Pb^{2+} adsorption onto P15DAN particles based on Fig. 4a

Mathematical model	Equation	Correlation coefficient	Standard deviation	h' (mg·g^{-1}·min^{-1})
Pseudo-first-order	$\mathrm{Log}\,(Q_e\text{-}Q_t) = -0.047\,t - 0.927$	0.7360	0.4579	
Pseudo-second-order	$t/Q_t = 0.01121\,t + 0.04594$	1.0000	0.01965	21.8
Lagergren	$Q_t = 90\,(1\text{-}e^{-3.7697\,t})$	0.9987	0.3487	

Table 6 An overview on the representative micro- and nanomaterial-based sorbents toward Pb(II) ions

Materials used	Pb(II) adsorption capacity ($mg \cdot g^{-1}$)	Reusability	Pb(II) adsorption selectivity	Preparation process	Integral cost-benefit	Refs.
Polyvinylbutyral microbead	86.2	Good	Good selectivity over Cd(II) and Cu(II)	Two-step	Low	[19]
P18DAN particles	116.0	Good	High selectivity over Na(I), K(I), Ca(II), Mg(II)	One-step, ambient air atmosphere, aqueous reaction medium	Low	This study
Mesoporous activated carbons	118.8	Good	NA	Multistep, energy-consuming (450 °C), environmentally harmful (H_3PO_4)	Low	[20]
Biorefinery waste of *Fucus spiralis*	132.0	Good	NA	Environmental benignity	Medium	[21]
Magnetic porous bio-adsorbent modified with amino siloxane	133.3	Excellent	Good selectivity over Ni(II), Cu(II), Co(II), Zn(II)	Sophisticated, multistep, environmentally harmful	Low	[22]
Ball-milled wheat straw-biochar	134.7	NA	NA	Two-step, energy-consuming (600 °C)	Medium	[23]
Ethylenediamine treated polyhydroxyethyl methacrylate microspheres	136.2	NA	Good selectivity over Cu(II)	Two-step	Medium	[24]
Chelating polyacrylonitrile beads	145.0	Good	Medium selectivity over Cd(II)	Two-step	Medium	[25]
Co-γ-Fe_2O_3 nanomaterials	154.9	Excellent	NA	Single-step hydrothermal synthesis at 180 °C	Medium	[26]
Potato peel-based activated carbon	167.0	NA	NA	Multistep, energy-consuming (600 °C in 99.999% N_2), environmentally harmful (H_3PO_4)	Low	[5]
Dithiocarbamate-anchored polymer/organosmectite composites	170.7	Good	Medium selectivity over Cd(II) & Cr(III)	Multistep, environmentally harmful (CS_2)	Medium	[27]
Hexamethylenediamine treated polyhydroxyethyl methacrylate microspheres	174.2	NA	Good selectivity over Cu(II)	Two-step	Medium	[24]
Magnetic biochar based on persulfate-Fe^0 treated sludge	180.0	Good	Good selectivity over Cd(II), Ni(II), Zn(II) but not Cu(II)	Two-step, energy-consuming (600 °C)	Medium	[28]
Rice straw biochar	198.2	NA	NA	Single step, energy-consuming (700 °C)	Medium	[29]
Ladle furnace steel (CaO & SiO_2) dust	208.9	NA	NA	Environmental benignity	High	[30]
Polyacrylamide grafted Fe_2O_3	211.4[a]	Good	Slight selectivity over Hg(II), Cd(II)	Multistep	Medium	[31]
Maleic anhydride modifying walnut shell	221.2[a]	Good	NA	Single step	High	[32]
Microporous titanosilicate	231.8[a]	NA	Medium selectivity over Na(I), K(I), Cd(II), Cu(II) & Zn(II)	Two-step, environmentally harmful (TiF_4)	Medium	[33]
Thiol-functionalized activated carbon from sewage sludge/coal blending	238.1[a]	NA	Medium selectivity over Cd(II), Cu(II), Ni(II)	Multistep, energy-consuming (500–800 °C), environmentally harmful ($HSCH_2COOH$)	Medium	[3]
Fe_3O_4@1,8-dihydroxyanthraquinone functionalized GO nanocomposite	243.1[a]	Good	Good selectivity over Cd(II), Co(II), Zn(II), Ni(II)	Sophisticated, multistep, environmentally harmful (H_2SO_4)	Medium	[34]
Banana peels-biochar	247.1[a]	NA	Medium selectivity over Cu(II), Cd(II)	Two-step, energy-consuming (600 °C)	Medium	[35]
Mesoporous silica-grafted GO	255.1[a]	NA	High selectivity over Li(I), Na(I), K(I), Ca(II), Mg(II), Cd(II), Cr(III), Co(II), Hg(II), As(III), Mn(II), Ni(II), Zn(II)	Sophisticated, multistep, environmentally harmful (H_2SO_4)	High	[6]
Hybrid macroporous modified silica	256.7[b]	Medium	Medium selectivity over Hg(II)	Sophisticated, multistep, environmentally harmful ($(CH_3O)_3Si(CH_2)_3SH$, $HS(CH_2)_2SO_3H$, and $HS(CH_2)_3SO_3H$)	High	[4]
P15DAN microparticles	241.0[b] 265.3[a]	Good	High selectivity over Na(I), K(I), Mg(II), Ca(II)	One-step, ambient temperature/air atmosphere, neutral aqueous reaction medium	High	This study

[a] By Langmuir equation

[b] Experimental values

data through a regression analysis. The parameters and the correlation coefficients are listed in Table 4. It is obvious that the results show that the adsorption behavior of Pb^{2+} ions on P15DAN particles can be better expressed by the Langmuir isotherm than Freundlich and Temkin isotherms because Langmuir model yields a higher correlation coefficient. Moreover, the saturated Pb^{2+} adsorbance can be estimated to be 265.3 $mg{\cdot}g^{-1}$ by Langmuir simulation.

Effect of solution pH on Pb^{2+} adsorption: The effect of pH on Pb^{2+} adsorption onto P15DAN particles is shown in Fig. 4b by adding a certain amount of 50 mM HNO_3 or CH_3COONa. It is interesting that the adsorbance and adsorptivity of Pb^{2+} ions keep the highest values despite the variation of pH value in the range of 2.0 to 6.0. In this case, the predominant chelation adsorption between the Pb^{2+} and amino/imino groups on P15DAN is more stable but not affected by the pH value. A sharp diminution in the Pb^{2+} adsorbability is observed in a pH range from 6 to 6.9. It can be speculated that the lead ions may have lower mobility and solubility in higher pH solution. Consequently, the P15DAN particles may have less probability of collision with the Pb^{2+} ions.

Regeneration of the P15DAN microparticles

The P15DAN microparticles adsorbing Pb(II), Hg(II), and Ag(I) can directly be regenerated. The complexed Pb(II), Hg(II), and Ag(I) ions on the microparticles can be desorbed and thus regenerated with 0.5 M HNO_3 as desorbent. It seems that the regeneration step slightly affects its following adsorbability [17, 18]. The reduced element Hg and Ag metals on the microparticles can be recovered by centrifugation of their aqueous dispersion, accompanying by the regeneration of the microparticles [15]. This is perhaps useful to take a pragmatic view on this work.

Comparison of Pb^{2+} adsorption onto the P15DAN particles with other sorbents: As discussed above, the experimentally highest Pb^{2+} adsorbance is found to be 241 $mg{\cdot}g^{-1}$ for P15DAN. Furthermore, the theoretically maximal Pb^{2+} adsorption capacity can be 265.3 $mg{\cdot}g^{-1}$ for P15DAN by Langmuir simulation. An overview on the typical micro- and nanomaterial-based sorbents and other representative sorbents toward Pb(II) ions has been summarized in Table 6. Although it is hard to directly compare the P15DAN with other adsorbents due to different adsorption conditions, the thiol-functionalized activated carbon, functionalized GO, biochar, porous modified silica, and P15DAN may have the strongest Pb(II) adsorbability. Note that the former four materials were prepared by a relatively sophisticated two- or multi-step procedure sometimes including energy-consuming or environmentally harmful stages. This brings on relatively low productivity, relatively weak cost-effectiveness, and little environmental benefit in the case of Pb(II) decontamination for environmental purification. It should be noticed that the preparation of the P15DAN microparticles by a one-step chemical oxidative precipitation polymerization of 15DAN in neutral aqueous reaction medium at room temperature in ambient air atmosphere is readily, highly efficient, and scalable. Furthermore, the P15DAN microparticles possess the strong resistance to water, aqueous acid and alkali, and odorlessness. All of these features demonstrate that the P15DAN microparticles would have an important potential of application as a highly integral cost-beneficial Pb^{2+} adsorbent for the elimination and recovery of toxic Pb^{2+} from its polluted wastewaters.

Conclusions

The chemical oxidation polymerization of 1,5-diaminonaphthalene in a mixture of equal volume of acetonitrile and water with ammonium persulfate as oxidant at ambient temperature in ambient air has successfully generated fine P15DAN microparticles with a high yield and productivity. The structure, properties and functionality of the P15DAN microparticles can be significantly optimized by adjusting the oxidant/monomer ratio and also oxidant species. The microparticles at $(NH_4)_2S_2O_8$/15DAN molar ratio of 1/2 possess the longest π-conjugated length, while the microparticles at $(NH_4)_2S_2O_8$/15DAN ratio of 1/1 exhibit the highest Pb^{2+} adsorbability by a dominant chelation between Pb^{2+} and amino/imino groups. The Pb^{2+} adsorption consists of two steps, the first fast reactive adsorption on the particle surface and the second slow interior adsorption inside the particles. The Pb^{2+} adsorption capacity of 241 $mg{\cdot}g^{-1}$ (P15DAN) is slightly lower than theoretical capacity (265.3 $mg{\cdot}g^{-1}$) by Langmuir simulation but higher than those on most of other sorbents including P18DAN, though the P18DAN possesses stronger Hg^{2+} and Ag^{+} adsorbability than P15DAN. The P15DAN microparticles formed by $(NH_4)_2S_2O_8$ exhibit strong resistance to aqueous HCl and NaOH, but much lower resistance to organic solvents. On the contrary, the solubility of the P15DAN in highly polar solvents including NMP, DMSO, and DMF signifies its solution processability. The P15DAN particles as a new cost-effective sorbent are very useful in collection and removal of lead/mercury/silver ions from water effluents without highly polar organic solvents, simultaneously achieving water decontamination and purification.

Acknowledgements We thank the Shenzhen Fundamental Research Project of China (JCYJ20160318095112976), the JSPS Invitational Fellowship for Research in Japan (ID No. L18516), and the National Natural Science Foundation of China (51273148). We are grateful to Professors Hiroshi Imahori, Tomokazu Umeyama, Tomohiro Higashino, and Ms. Naoko Nishiyama at Kyoto University for their important helps.

Compliance with ethical standards The author(s) declare that they have no competing interests.

References

1. Das R, Giri S, King Abia AL, Dhonge B, Maity A (2017) Removal of Noble metal ions (ag^+) by Mercapto group-containing Polypyrrole matrix and reusability of its waste material in environmental applications. ACS Sustain Chem Eng 5:2711–2724
2. Deng S, Zhang G, Liang S, Wang P (2017) Microwave assisted preparation of thio-functionalized polyacrylonitrile fiber for the selective and enhanced adsorption of mercury and cadmium from water. ACS Sustain Chem Eng 5:6054–6063
3. Li J, Xing X, Li J, Shi M, Lin A, Xu C, Zheng J, Li R (2018) Preparation of thiol-functionalized activated carbon from sewage sludge with coal blending for heavy metal removal from contaminated water. Environ Pollution 234:677–683
4. Schroden RC, Al-Daous M, Sokolov S, Melde BJ, Lytle JC, Stein A, Carbajo MC, Fernandez JT, Rodríguez EE (2002) Hybrid macroporous materials for heavy metal ion adsorption. J Mater Chem 12:3261–3267
5. Kyzas GZ, Bomis G, Kosheleva RI, Efthimiadou EK, Favvas EP, Kostoglou M, Mitropoulos AC (2019) Nanobubbles effect on heavy metal ions adsorption by activated carbon. Chem Eng J 356:91–97
6. Li X, Wang Z, Li Q, Ma J, Zhu M (2015) Preparation, characterization, and application of mesoporous silica-grafted graphene oxide for highly selective lead adsorption. Chem Eng J 273:630–637
7. Al Hamouz OCS, Adelabu IO, Saleh TA (2017) Novel cross-linked melamine based polyamine/CNT composites for lead ions removal. J Environ Manag 192:163–170
8. Li XG, Huang MR, Duan W, Yang YL (2002) Novel multifunctional polymers from aromatic diamines by oxidative polymerizations. Chem Rev 102:2925–3030
9. Huang MR, Lu HJ, Li XG (2012) Synthesis and strong heavy-metal ion sorption of copolymer microparticles from phenylenediamine and its sulfonate. J Mater Chem 22:17685–17699
10. Li XG, Zhang JL, Huang MR (2012) Interfacial synthesis and functionality of self-stabilized Polydiaminonaphthalene nanoparticles. Chem Eur J 18:9877–9885
11. Li XG, Dou Q, Huang MR (2008) Titrimetric analysis of total mercury ions including mercury (I) ions. Monatshefte für Chemie-Chemical Monthly 139(10):1157–1162
12. Li XG, Huang MR, Li SX (2004) Facile synthesis of poly(1,8-diaminonaphthalene) microparticles with a very high silver-ion adsorbability by a chemical oxidative polymerization. Acta Mater 52:5363–5374
13. Huang MR, Ding YB, Li XG, Liu Y, Xi K, Gao CL, Kumar RV (2014) Synthesis of semiconducting polymer microparticles as solid ionophore with abundant complexing sites for long-life Pb(II) sensors. ACS Appl Mater Interfaces 6(24):22096–22107
14. Huang MR, Li S, Li XG (2010) Longan shell as novel biomacromolecular sorbent for highly selective removal of lead and mercury ions. J Phys Chem B 114(10):3534–3542
15. Li XG, Feng H, Huang MR (2009) Strong adsorbability of mercury ions on aniline/sulfoanisidine copolymer nanosorbents. Chem Eur J 15(18):4573–4581
16. Kumar TM, Achar BN (2006) Synthesis and characterization of lead phthalocyanine and its derivatives. J Organomet Chem 691: 331–336
17. Huang MR, Lu HJ, Li XG (2007) Efficient multicyclic sorption and desorption of lead ions on facilely prepared poly(m-phenylenediamine) particles with extremely strong chemoresistance. J Colloid Interface Sci 313:72–79
18. Huang MR, Lu HJ, Song WD, Li XG (2010) Dynamic reversible adsorption and desorption of lead ions through a packed column of poly(m-phenylenediamine) spheroids. Soft Mater 8:149–163
19. Denizli A, Tanyolaç D, Salih B, Özdural A (1998) Cibacron blue F3GA-attached polyvinylbutyral microbeads as novel magnetic sorbents for removal of cu(II), cd(II) and Pb(II) ions. J Chromatogr A 793:47–56
20. Huang Y, Li S, Chen J, Zhang X, Chen Y (2014) Adsorption of Pb (II) on mesoporous activated carbons fabricated from water hyacinth using H3PO4 activation: adsorption capacity, kinetic and isotherm studies. Appl Surf Sci 293:160–168
21. Filote C, Volf I, Santos SC, Botelho CM (2019) Bioadsorptive removal of Pb (II) from aqueous solution by the biorefinery waste of Fucus spiralis. Sci Total Environ 648:1201–1209
22. Zhou J, Liu Y, Zhou X, Ren J, Zhong C (2018) Magnetic multiporous bio-adsorbent modified with amino siloxane for fast removal of Pb(II) from aqueous solution. Appl Surface Sci 427:976–985
23. Cao Y, Xiao W, Shen G, Ji G, Zhang Y, Gao C, Han L (2019) Carbonization and ball milling on the enhancement of Pb(II) adsorption by wheat straw: competitive effects of ion exchange and precipitation. Bioresour Technol 273:70–76
24. Denizli A, Salih B, Pişkin E (1997) New sorbents for removal of heavy metal ions: diamine-glow-discharge treated polyhydroxyethylmethacrylate microspheres. J Chromatogr A 773:169–178
25. Bhunia P, Chatterjee S, Rudra P, De S (2018) Chelating polyacrylonitrile beads for removal of lead and cadmium from wastewater. Sep Purif Technol 193:202–213
26. Chen W, Lu Z, Xiao B, Gu P, Yao W, Xing J, Asiri AM, Alamry KA, Wang X, Wang S (2019) Enhanced removal of lead ions from aqueous solution by iron oxide nanomaterials with cobalt and nickel doping. J Clean Prod 211:1250–1258
27. Say R, Birlik E, Denizli A, Ersöz A (2006) Removal of heavy metal ions by dithiocarbamate-anchored polymer/organosmectite composites. Appl Clay Sci 31:298–305
28. Ho SH, Wang D, Wei ZS, Chang JS, Ren NQ (2018) Lead removal by a magnetic biochar derived from persulfate-ZVI treated sludge together with one-pot pyrolysis. Bioresour Technol 247:463–470
29. Shen Z, Hou D, Jin F, Shi J, Fan X, Tsang DC, Alessi DS (2019) Effect of production temperature on lead removal mechanisms by rice straw biochars. Sci Total Environ 655:751–758
30. Bouabidi ZB, El-Naas MH, Cortes D, McKay G (2018) Steelmaking dust as a potential adsorbent for the removal of lead (II) from an aqueous solution. Chem Eng J 334:837–844
31. Manju GN, Krishnan KA, Vinod VP, Anirudhan TS (2002) An investigation into the sorption of heavy metals from wastewaters by polyacrylamide-grafted iron(III) oxide. J Hazard Mater B 91: 221–238

32. Li S, Zeng Z, Xue W (2018) Adsorption of Lead ion from aqueous solution by modified walnut Shell: kinetics and thermodynamics. Environ Technol. https://doi.org/10.1080/09593330.2018.1430172
33. Zhao GX, Lee JL, Chia PA (2003) Unusual adsorption properties of microporous titanosilicate ETS-10 toward heavy metal lead. Langmuir 19:1977–1979
34. Khazaei M, Nasseri S, Ganjali MR, Khoobi M, Nabizadeh R, Gholibegloo E, Nazmara S (2018) Selective removal of lead ions from aqueous solutions using 1,8-dihydroxyanthraquinone (DHAQ) functionalized graphene oxide; isotherm, kinetic and thermodynamic studies. RSC Adv 8:5685–5694
35. Ahmad Z, Gao B, Mosa A, Yu H, Yin X, Bashir A, Ghoveisi H, Wang S (2018) Removal of cu(II), cd(II) and Pb(II) ions from aqueous solutions by biochars derived from potassium-rich biomass. J Clean Prod 180:437–449